Nonlinear Identification in the DISCOS Position Sensor

P. A. Yansouni*
Ecole Polytechnique, Montreal Canada
and
D. B. DeBra†
Stanford University, Stanford, Calif.

The electric null of the position sensor of a drag-free satellite[1] is expected to change its location with respect to the geometrical center of the sensor due to aging. This offset creates an increasing nonlinearity in the sensor's response, causing distortion of the output signal. A technique has been developed to identify the amount of null offset from samples of the output signal only when the disturbances on the satellite are relatively constant. A linearized least squares fit is used. Difficulties are caused by parameter equivalence of first order and data noise near the center; however, accurate estimation can be obtained for large null offset.

Introduction

A SATELLITE in orbit is perturbed by two major sources, residual air drag and solar pressure. DISCOS (Disturbance Compensation System) is a control system designed to insure that a satellite's trajectory is determined by gravity forces only, thus eliminating orbital changes caused by the perturbations. Interesting applications of DISCOS to navigation, aeronomy, and geodesy have been reported.[1,2] DISCOS was launched on the TRIAD Satellite on September 2, 1972.

In DISCOS, a small sphere about the size of a ping pong ball—referred to as "proof mass"—is free to move in a hollow cavity inside the satellite's main body, and is therefore shielded from external disturbances. The relative motion between the two bodies is sensed, and gas jets are actuated to constrain the main body of the satellite to follow the proof mass without touching it. The proof mass is located in a spherical shell which has three pairs of plates diametrically opposed and electrically isolated. When a relative motion occurs, the change in capacity between each pair of plates is measured (see Fig. 1), and the control system causes gas jets to fire so as to re-establish the vehicle in its proper location, following the proof mass. This position sensor is called a capacitive pickoff.

The most important internal disturbing forces are the mass attraction between the proof mass and the satellite, and the electrostatic forces caused by the pickoff. Ideally, the main body center of mass—the center of geometry of the capacitor shell—and the proof mass center are in the same location. In addition, parts are located and compensating masses added to eliminate the mass attraction force and its gradient,[3] which minimizes this error. Symmetry also minimizes electrostatic forces. The electric null of the sensor must be located at the center of the pickoff for these errors to remain small. However, because of the aging of the electronic components and changes in the shunt capacity of the circuitry, the electric null may drift. It is therefore desirable to have a way of identifying on orbit the pickoff null location with respect to the spherical shell. Considerations in bounding the null shift include:

a) The ball must not hit the wall if the system is to operate. To maintain adequate sensitivity, the difference in radius between the proof mass and the shell is only 9.5 mm. The null shift must be less.

b) The average location of the proof mass must be within 1 mm of the compensated location to keep the net mass attraction forces exerted by the satellite's main body on the proof mass within the DISCOS specification of $10^{-11}g$. This effect is the consequence of the nonspherical distribution of mass in the main body, and our inability to make the gradient smaller. For a quantitative discussion and the methods of minimizing the gradient, see Ref. 3.

c) If the proof mass is closer to one wall, there will be an unbalanced electrostatic force due to the sensor excitation. For low voltage, it can be smaller in magnitude than the mass attraction forces. However, electrostatic charge buildup on the proof mass could make it more significant.[1]

d) The null offset, combined with small uncertainties in the location of the center of mass with respect to the geometrical center of the pickoff, results in a dynamic coupling between the attitude and translational control system reducing the margins of stability.[4,5]

The gas jets' control law is a simple derived rate mechanization.[6] To reduce fuel consumption, a deadband is provided (2 mm total width in the flight sensor), and all relative motions used in this analysis take place within the deadband.

Let e_c be the characteristic voltage of the pickoff vs displacement x_c, x_s be the null shift, and x the relative motion with respect to the null. Figure 2 illustrates the sensor characteristic changed by the null shift from which $x_c = x_s + x$. The nonlinearity of the portion of the characteristic within the deadband causes output-signal distortion.

If the ball plate capacitance in Fig. 1 is modeled by a parallel plate capacitance, and the resistors impedance neglected with respect to the impedance of the capacitors, it can be shown that the output voltage e_c is related to x_c by

$$e_c = \frac{kx_c}{a^2 - x_c^2} = f(x_c) \tag{1}$$

where a is nominally the distance between a plate and the ball when centered (virtual gap), and k is a factor of proportionality. This form has been found to be an accurate analytical model of the sensor's characteristic.

Since the identification procedure is based on the nonlinear distortion of the signal, the model's curvature must ap-

Presented as Paper 74-904 at the AIAA Mechanics and Control of Flight Conf., Anaheim, California, Aug. 1974; submitted October 21, 1974; revision received September 2, 1975. Research partially supported by Johns Hopkins University, Applied Physics Laboratory, under Contract APL/JHU 271881.

Index categories: Spacecraft Navigation, Guidance, and Flight-Path Control Systems; Navigation, Control, and Guidance Theory.

*Associate Professor, Department of Electrical Engineering.

†Professor of Aeronautics and Astronautics, and Mechanical Engineering; Director, Guidance & Control Laboratory. Fellow, AIAA.

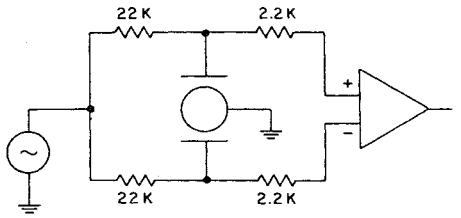

Fig. 1 Simplified representation of the pickoff circuit.

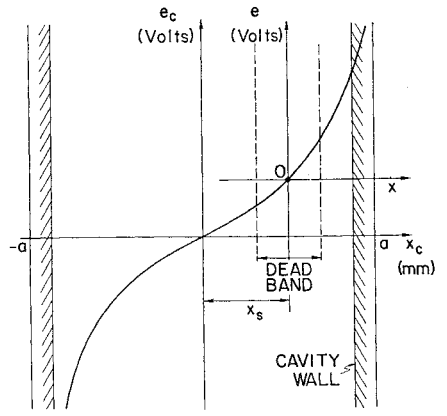

Fig. 2 Representation of the null shift on the pickoff characteristic.

proximate closely the curvature of the pickoff characteristic. The analytical expression for the output voltage when the null has shifted by an amount x_s is

$$e(x,x_s) = f(x+x_s) - f(x_s) \tag{2}$$

Expansion of $e(x,x_s)$ in a power series of x and simple numerical evaluation for typical pickoff parameters show that the third and higher terms in the expansion are less than 1% of the linear term[7] over the whole range of possible values of x and x_s. Consequently, $e(x,x_s)$ is adequately represented by

$$e(x,x_s) = \frac{k(a^2+x_s^2)}{(a^2-x_s^2)^2}\, x + \frac{kx_s(3a^2+x_s^2)}{2(a^2-x_s^2)^3}\, x^2 \tag{3}$$

If the nonlinearity of the pickoff were neglected, the gain of the pickoff, the null shift, and the amplitude of motion would have interchangeable effects of the output signal, thus eliminating any possibility of separate identification.

In the actual pickoff, the resistors (Fig. 1) limit the current in the capacitance, and the parameter a loses its immediate geometrical significance (plate to ball). In the three-dimensional pickoff, coupling between the channels is created by the spherical shape. The mathematical model accounting for the coupling at centered null for the x axis is

$$e_x = f(x,0)\,[1 + b_x(y^2+z^2)] \tag{4}$$

The coefficient b_x accounts for the coupling. Analogous expressions for channels y and z are obtained by cyclical permutation of the variables.

For the laboratory two-dimensional simulator,[7] built to develop and test DISCOS, the expression analogous to Eq. (4) is

$$e_x = f(x,0)\,[1 + b_x y^2] \tag{5}$$

Parameter values were obtained by least squares fitting to data taken in the laboratory. The results for both models are summarized in Tables 1 and 2.

Table 1 Simulator's pickoff parameters

x Axis	y Axis	Units
$k = 58.25$	$k = 51.74$	10^{-2} V in.
$a = 12.86$	$a = 12.46$	10^{-2} in.
$b = 0.0081$	$b = 0.0079$	100 in.$^{-2}$

Table 2 Satellite pickoff parameters

x Axis	y Axis	z Axis	Units
$k = 15.126$	$k = 18.123$	$k = 15.911$	10^{-2} V in.
$a = 40.07$	$a = 40.83$	$a = 40.27$	10^{-2} in.
$b = 2.10^{-2}$	$b = 2.10^{-2}$	$b = 2.10^{-2}$	100 in.$^{-2}$

Data Formats and Uncertainties

The output data are used in a sampled form. They include noise, and the object of this section is to determine roughly the proportion of noise in the measurements and its degree of correlation.

Laboratory Data

The simulator's pickoff output is an analog signal. It was recorded on paper and amplitudes were measured directly on the graph for discrete values of time. Typical peak-to-peak amplitudes of the motion were around 0.01 mm (0.4×10^{-3} in) corresponding to a signal amplitude of about 30 mV. The variance of the cumulative error due to reading accuracy and noise in the measurements was estimated at less than 5% of the signals' peak-to-peak amplitude. Inspection of noise frequencies with respect to the sampling interval substantiate the claim that noise samples were uncorrelated.

Flight Data

The analog signals corresponding to the DISCOS' three axes are sampled in the spacecraft and transmitted to the ground via three telemetry channels. The sampling interval is 5 sec and the three signals are sampled consecutively with a delay of 0.08 sec between channels. The small amplitude error introduced by the delay is estimated at 0.13% of the signal's peak-to-peak amplitude and therefore neglected. The data are quantized for digital transmission with an 8-bits accuracy. Since the analog range is 500 mV, the quantization step is approximately 2 mV.

Actual flight data show that the signal's amplitude is of the order of 40 mV corresponding to motions of about 1 mm if the pickoff gain has its nominal value, which implies that little or no shift of the null has occurred. At times, the flight data depart significantly from the parabolic shape expected for the related motion of the satellite with respect to the proof mass. This error is caused by thermal effects in passing between shadow and sunlight, causing boom bending and displacement of the pickoff center with respect to the satellite mass center. In the rest of the data, noise comes from two major sources: the bending modes of the booms excited by the jets firing, and the quantization noise. Since the quantizer is symmetric, and the signal range several times the quantization step, the quantization noise can be considered uncorrelated with zero average and a variance equal to the quantization step over the square root of 12, i.e., less than 1 mV.[8] The boom bending period is about 20 sec and results in a sinusoidal error in the data with a peak-to-peak amplitude ranging from 4-8 mV. Only the least noisy data were selected for processing: 6 parabolas per channel, each spanning an average 200 sec with amplitudes ranging from 20-30 mV. Though DISCOS operated for nearly a year before being turned off, only a few weeks of the pickoff data were recorded before telemetry was lost six weeks after launch.

Formulation and Analysis

The analytic formulation of the fitting procedure is best detailed on a one-dimensional sensor. Extension to the three-dimensional case is straightforward. Assume a constant disturbance (constant drag and solar pressure between firings of the gas jets).

With respect to the proof mass, the motion $x(t)$ of the satellite is

$$x(t) = \ddot{x}_0 t^2 + \dot{x}_0 t + x_0 \tag{6}$$

where $\ddot{x}_0 \equiv$ constant acceleration due to perturbation forces, $\dot{x}_0 \equiv$ initial velocity after firing, and $x_0 \equiv$ initial position after firing.

Let n be the number of samples available for each parabolic arc, and e_m be an $n \times 1$ array where the samples are stored; m the number of parameters to be identified, and p an $m \times 1$ array where the current estimates of these parameters are stored; e is an $n \times 1$ array containing the computed output of the sensor at the same sampling times, using the parameter values in p; S_q the sum of the squares of the components of $e_m - e$. The pickoff gain k and the null shift x_s are included in p with the parameters in Eq. (6).

$$p \equiv [k, x_p, \ddot{x}_0, \dot{x}_0, x_0] \tag{7}$$

$$S_q \equiv (e_m - e)^T (e_m - e) \tag{8}$$

The problem is to find the value of p that minimizes S_q. This value of p verifies the equation $(\partial S_q)/(\partial p) = 0$. Given the nonlinear structure of the model, however, this equation is not practical to solve directly. Minimization of S_q with respect to p has been attempted via several minimum seeking techniques; i.e., random searches, perturbation technique, gradient, and iterative least squares. The first two resulted in a poor rate of convergence and poor accuracy, the gradient showed a better accuracy but a very slow rate of convergence when close to the minimum. Best results were obtained using the standard iterative least squares method described in the following.

Let $\bar{p}$ be the current estimate of p_a, the actual set of parameters, and $p_a = \bar{p} + \delta p$. Denoting by A the $n \times 1$ matrix $\partial e/\partial p \,|\bar{p}$, and approximating $e(p_a)$ by the two first terms in its Taylor expansion around $\bar{p}$ yields

$$S_q . (e_m - \bar{e} - A\delta p)^T (e_m - \bar{e} - A\delta p) \tag{9}$$

The minimizing value of δp can be computed using the necessary condition, $\partial S_q / \partial \delta p = 0$. It yields

$$\delta p = (A^T A)^{-1} A^T (e_m - \bar{e}) \tag{10}$$

The increment δp is added to $\bar{p}$ and the procedure is repeated with $\bar{p} + \delta p$ as the new estimate of p_a until convergence is attained. Note that this method is equivalent to a second-order gradient algorithm and has its covergence properties.

The procedure fails completely if the $m \times m$ matrix $A^T A$ is not full rank. This occurs if $n < m$, less measurements than parameters, or if some of the parameters are equivalent in their effect on e, in which case some columns of A differ only by a scalar factor. This is the case when $x_s = 0$. Even for the actual value of x_s different from zero, if the starting value of $\bar{x}_s$ is taken equal to zero, the procedure fails. The remedy is to minimize the auxiliary function

$$J = (e_m - \bar{e} - A\delta p)^T (e_m - \bar{e} - A\delta p) + \delta p^T W \delta p \tag{11}$$

where W is an $m \times m$ positive definite diagonal matrix. The minimizing increment δp is

$$\delta p = (A^T A + W)^{-1} A^T (e_m - \bar{e}) \tag{12}$$

A rational way of choosing W is found in the interpretation of $\delta_p^T W \delta_p$ as a penalty imposed upon large variations of δp. Therefore, each term of the diagonal is to be taken inversely proportional to the estimated standard deviation of the error between the initial guess on the respective term of $\bar{p}$ and its actual value. For most parameters, a rough estimation can be obtained from the flight data and past information. If this estimate is unavailable at the initial stage, for x_s in particular, the standard deviation can be replaced by the maximum possible excursion of the parameters, i.e., for x_s it will be the gap between proof mass and cavity walls. The amplitude of W affects considerably the rate of convergence and had to be changed in the course of the minimization procedure.

The minimum seeking procedure converges to the nearest local minimum. With the model's structure, it so happens that two minima exist in the range of possible values for parameters x_s, $\ddot{x}_0$, $\dot{x}_0$, and x_0. One of them corresponds to the actual values of these parameters, the other to an almost symmetric value of x_s with respect to the origin, while the other parameters remain close to their nominal values. When noise is included in the measurements these minima cannot be distinguished by their relative amplitude, which depends essentially on the particular sample of noise taken with the measurements. It is still possible, however, to identify each minimum because of different patterns in the residuals $(e_m - \bar{e})$ when convergence is attained. In the absence of noise, fitting the model to the data at the auxiliary minimum will result in a finite error and a definite pattern in the residuals, as illustrated in Fig. 3.

From one parabola to another, these patterns will reproduce themselves almost identically. If, however, convergence has been attained with the actual set of parameters, the residuals will tend to zero with the number of iterations. Simple inspection of the residuals to differentiate between the actual and auxiliary minima is not possible because of the noisy data. It was shown[7] that by accumulating consecutively the residuals obtained, after fitting several arcs of parabolas to the model, a detection technique based on the residuals' statistical properties could be applied to extract the patterns from the noise when they existed. This method allows the successful separation of the actual and auxiliary sets of parameters as demonstrated by the detailed examples of Ref. 7.

Simulation and Laboratory Results

The estimation procedure was evaluated two ways using computer simulated data and experimental data with known null shifts on the laboratory version of DISCOS.

Computer simulated data were generated using the one-dimensional model with the gain k and the "virtual gap" a of the laboratory pickoff. Motion amplitudes were about 0.01 mm and x_s ranging from zero to 1.5 mm. The resulting signal's amplitude (when $x_s = 0$) was about 25 mV to which white noise was added with a variance $\sigma = 2$ mV. Several arcs of parabolas were generated for each value of x_s. $E\{x_w\}$ was estimated by averaging the results obtained from each set of parabolas, and the standard deviation (σ_{x_c}) evaluated by averaging $[x_s - E\{x_s\}]^2$. Figure 4 is a plot of $E\{x_s\}$ and σ_{x_s}. The norm of the relative error on x_s vs x_s is plotted in Fig. 5.

In order to extrapolate these results to other cases where parameters, motion amplitudes, and noise levels are different, Eq. (3) is rewritten as a function of nondimensional variables, expressed as a fraction of the virtual gap "a": $\xi = x/a$, $\eta = x_s/a$

$$e(a\xi, a\gamma) = \frac{k}{a} \frac{1+\eta^2}{[1-\eta^2]^2} \xi + \frac{k}{a} \frac{3+\eta^2}{(1-\eta^2)^3} \eta\xi^2 \tag{13}$$

Since only the second term on the right-hand side of Eq. (13) accounts for the nonlinearity of the pickoff, it is assumed that

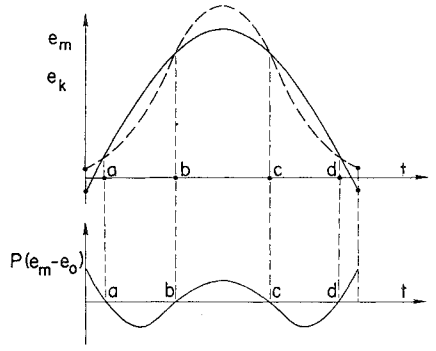

Fig. 3 Pattern in the residuals corresponding to the fit at the auxiliary minimum.

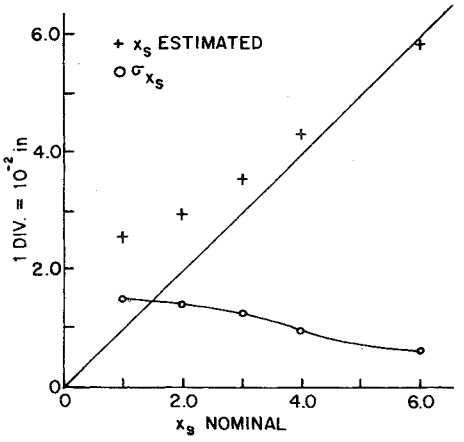

Fig. 4 Estimated values of x_s, and standard deviation vs nominal value of x_s.

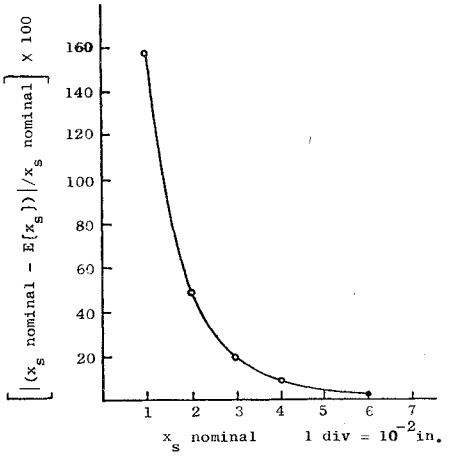

Fig. 5 Relative error vs x_s nominal.

the accuracy of the estimation procedure depends on the ratio of this term over the noise amplitude σ_v. Let

$$R=\frac{1}{\sigma_v}\cdot\frac{k}{a}\cdot\frac{3+\eta^2}{(1-\eta^2)^3}\,\eta\xi^2 \tag{14}$$

where R is dimensionless and is a measure of the "detectability" of the null shift in the presence of noise. Its usefulness is based on the assumption that in each case where R has the same value, the estimation results will be comparable in accuracy. A plot of R vs η is given in Fig. 6 with the values of ξ and σ_v used in the simulation. Since R increases with η, it appears that the larger the null shift, the better the accuracy of the estimation. In reality, this is not true because

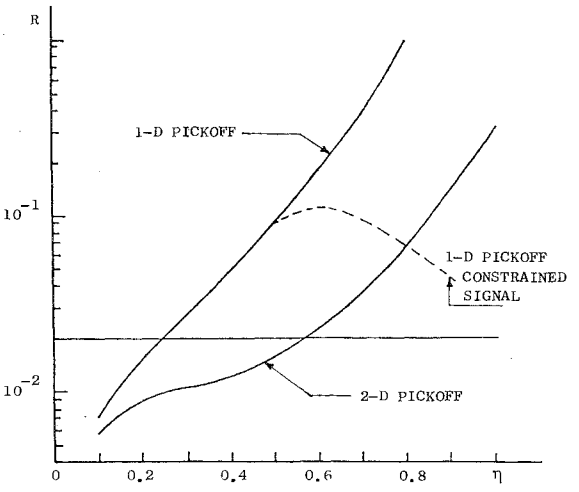

Fig. 6 Accuracy ratio vs normalized null shift.

the signal amplitude is constrained to the deadband width. Therefore, when the signal reaches its maximum amplitude, any increase in η corresponds to a decrease in the amplitude of the motion actually detected. Therefore, R reaches a maximum and decreases for large η. As an example, R has been plotted in Fig. 6 with a signal amplitude constrained to 40 mV, and ξ and σ_v having the same values as previously listed; however, when $e(\xi,\eta)$ reaches 40 mV, the effective ξ is computed from Eq. (13). The level of R for the accuracy to be acceptable is determined from the simulation results. The level of R corresponding to a 20% relative error on x_s is 2×10^{-2} and is indicated in Fig. 6. For different geometry, if an estimate of ξ is available, R could be computed for each η and by comparison to the level in Fig. 6 the range of detectable null shifts could be determined.

In the case of the two- and three-dimensional pickoffs, the accuracy deteriorates because of the coupling between channels. As a worst case analysis, the contribution of cross-axis motions to the output of each channel is considered as noise to be added to σ_v. As an example, if Eq. (4) is used for the pickoff model, the contribution of the motion along y and z to the output along x is to the first order

$$2a_3a^2\cdot\frac{k}{a}\cdot\frac{\eta}{1-\eta^2}\,(\gamma\lambda+\alpha\beta) \tag{15}$$

where

$$\gamma=y_s/a,\quad a=z_s/a,\quad \lambda=y/a,\quad \beta=z/a$$

To illustrate the effect of the coupling on the accuracy ratio, R has been computed for the two-dimensional simulator's pickoff. For this purpose, $y_s$and y have been assumed respectively equal to x_s and x and term Eq. (15) added to $\sigma_v(\alpha=\beta=0)$. R has been plotted in Fig. 6 (lower curve). The motion and noise level in the laboratory data are approximately the same as those used for the numerical simulation.

Tests of the technique were performed on data taken from the laboratory simulator of the drag-free satellite. The pickoff null was actually moved to an eccentric location corre-

Table 3 Estimated values of simulator's pickoff null location; unit of length is 10^{-2} in.

Parabola	x_s	y_s	(x_s) Nominal	(y_s) Nominal
1	2.44	6.85	0.025	6.01
2	2.26	6.81	0.025	6.01
3	2.39	6.80	0.025	6.01

Table 4 Flight data processing results

Set	$x_2 10^{-2}$in.(mm)	$\eta = x_s/a$	$y_s 10^{-2}$in.(mm)	$\gamma = y_s/a$	$z_s 10^{-2}$in.(mm)	$\alpha = z_s/a$
1	4.3(1.1)	0.11	2.6(0.66)	0.06	11.0(-2.7)	0.27
2	-0.22(-0.05)	-0.005	-11.0(-2.7)	-0.27	7.4(1.87)	0.18
3	3.2(0.81)	0.08	-2.0(-0.50)	-0.05	-1.4(-0.35)	-0.03
4	2.3(0.58)	0.05	-2.1(-0.53)	-0.05	-8.2(-2.08)	-0.20
5	—	—	—	—	—	—
6	-2.6(-0.66)	0.06	-3.1(-0.78)	-0.07	-1.0(-0.25)	-0.02
7	-0.35(-0.08)	-0.008	1.2(0.30)	0.03	-3.8(-0.96)	-0.09
Average	1.05(0.26)	0.03	-2.4(-0.61)	-0.06	-3.0(-0.76)	-0.08
Lower bound to the approximate expected uncertainty.		0.15		0.15		0.15

sponding to $y_s = 60.1 \times 10^{-3}$ in. and $x_s = 0.2 \times 10^{-3}$ in. The pickoff model used is Eq. (5) and its parameter values are in Table 1. Motion amplitudes and noise levels were as discussed earlier. Three arcs of parabolas were selected from the data and null shift was estimated for each. The results are summarized in Table 3. Computing the accuracy ratio for y_s with the results obtained yields $R = 2.7 \times 10^{-2}$. Referring to Fig. 6, in order to obtain the corresponding value of the null shift, and to the simulation results, it can be seen that the relative error on y_s to be expected is around 10%, which compares with the actual 13% error of the estimation procedure.

Processing of the Flight Data

Extension of the technique outlined in the section on "Formulation and Analysis" to the three-dimensional case is straightforward. In the actual programming, it requires enlargement of the arrays e_m and p to include the $3 \times n$ measurements and the $3 \times m$ parameters characterizing the pickoff gain and the motion dynamics.

The pickoff nominal parameters in Table 2 were determined from rather sketchy data: the gain in the linear portion of the characteristic, and the voltages with the ball against the center of each plate. The coupling coefficient, a parameter depending only on the geometry of the sensor, was taken to be the same as in an earlier prototype with approximately the same dimensions.

A total of seven sets of parabolas (three per set) were selected from the available data, the rest of which included large perturbations due to thermal effects on the booms, and to the caging and uncaging of the proof mass. The number of points per parabola ranged from 35-50 (175-250 sec) and the usable amplitude averaged 30mV. Corresponding to 0.7 mm (28×10^{-3} in.) if the pickoff has its nominal gain. The noise level has been discussed previously.

In comparison to the simulator's pickoff, the flight sensor has a characteristic with an extended "linear" portion, resulting in less distortion of the signal. It was expected that this effect would be compensated by the motion amplitude which was approximately 70 times larger. In effect, neglecting the coupling, the accuracy ratio is larger than 10^{-1} for $0.1 \leq \eta \leq 0.6$ as shown in Fig. 7, which implies, by comparison to the results in Fig. 6, that null shifts in this range could be detected.

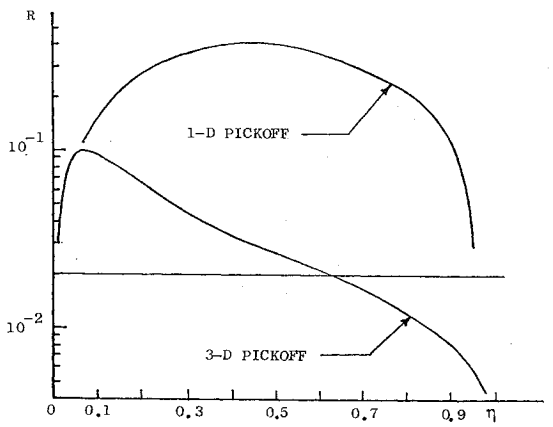

Fig. 7 Accuracy ratio vs null shift, with and without coupling.

As a cross check, a digital simulation of the flight pickoff was made and unfortunately the nondimensional results do not agree as well as it was hoped when compared on the basis of accuracy ratios, due to the large difference in the sensor's parameters. Application of the three-dimensional procedure to data generated numerically (with a noise level of $\sigma_v = 4$ mV) showed that the signal's amplitude must approach 100 mV before a null displacement with components along the three axis of 50, 150, 250×10^{-3} in., respectively (in the nondimensional form 0.13, 0.38, 0.63), could be detected with less than 20% relative error on each. Since the usable data have an amplitude no larger than 30 mV, the whole range of null displacements is below the detection level of the identification technique.

With the flight sensor geometry and noise levels, successful identification of the null shift requires a slight enlargement of the deadband (from 80-100 mV), and an increase in the gas jet impulses. Since the motion amplitude is proportional to the square of the initial velocity after each firing of the gas jets, the approximate threefold increase in the motion amplitude needed to utilize the whole width of the deadband could be obtained by multiplying the firing time of the gas jets by the square root of three. The results of the flight data processing are summarized in Table 4. The fitted values are all small compared with the estimated expected uncertainty and hence are not significant, viz.: there was no detectable null shift in the DISCOS position sensor.

References

[1] Lange, B. O., "The Drag-Free Satellite," *AIAA Journal*, Vol. 2, Sept. 1964, pp. 1590-1606.

[2] Space Dept. of the Johns Hopkins University, Applied Physics Lab. and the Guidance and Control Lab. of Stanford University, "A Satellite Freed of All But Gravitational Forces: 'TRIAD I'," *Journal of Spacecraft & Rockets*, Vol. 11, Sept. 1974, pp. 637-644.

[3] Fleming, A. and Tashker, M., "Final Report on Mass Attraction of TRIAD I/DISCOS," Contr. No. APL/JHU 271881, Sept. 1972, SUDAAR No. 445, Dept. Aeronautics and Astronautics, Stanford University, Stanford, Calif.

[4] Fleming, A. and DeBra, D.B., "The Stability of Gravity Stabilized Drag-Feee Satellites," *AIAA Journal*, Vol. 9, Oct. 1971, pp. 1980-1984.

[5] Fleming, A., DeBra, D. B., and Crespo di Silva, M., "Attitude-Translation Coupling in Drag-Free Satellites," *Proceedings of the Third IFAC Conference, Automatic Control in Space*, 1970.

[6] Nichlas, J. C. and Vivian, H. C., "Derived Rate Increment Stabilization: Its Application to the Attitude Control Problem," *Transactions of the ASME*, March 1962.

[7] Yansouni, P., "Data Processing for Pickoff Parameter Identification," Dept. Aeronautics and Astronautics, Stanford University, Stanford, Calif., SUDAAR No. 403, 1970.

[8] Widrow, B., "A Study of Rough Amplitude Quantization by Means of Nyquist Sampling Theorum," *Transactions of the P.C.G.T., CT-3, 1956.*